Peculiar corner states in magnetic fractals

Zhixiong Li [1] and Peng Yan [2,*]

[1] *School of Physics, Central South University, Changsha 410083, China*

[2] *School of Physics and State Key Laboratory of Electronic Thin Films and Integrated Devices, University of Electronic Science and Technology of China, Chengdu 610054, China*

(Received 26 March 2024; revised 23 May 2024; accepted 19 June 2024; published 1 July 2024)

Topological excitations in periodic magnetic crystals have received significant recent attention. However, their fate once the lattice periodicity is broken is an open question. In this paper, we theoretically study the topological properties embedded in the collective dynamics of magnetic texture array arranged into a Sierpiński carpet structure with effective Hausdorff dimensionality $d_f = 1.893$. By evaluating the quantized real-space quadrupole moment, we obtain the phase diagram supporting peculiar corner states that are absent in conventional square lattices. We identify three different higher-order topological states, i.e., outer corner state and type-I and II inner corner states. We further show that all these corner states are topologically protected and are robust against moderate disorder. Full micromagnetic simulations are performed to verify theoretical predictions with good agreement. Our results pave the way to investigating topological phases of magnetic texture based fractals and bridging the gap between magnetic topology and fractality.

DOI: 10.1103/PhysRevB.110.024402

I. INTRODUCTION

Due to the potential applications of topological insulators (TIs) in information transmission and quantum computing [1–3], researching the topological phase of matter has become one of the central topics in physics and engineering. Moreover, the discovery of higher-order TIs (HOTIs) [4–10] has further extended the scope of the topology family. In condensed matter physics, the natural and artificial materials are generally characterized in the context of crystals which consist of periodically arranged atoms with translational symmetry. The quantized topological invariants in momentum space can therefore be conveniently computed to describe the topological states, which constitutes the so-called *bulk-boundary* or *bulk-corner* correspondence [11–14]. Interestingly, there also exist some other materials which have ordered structure but do not support translational symmetry, such as quasicrystals [15,16] and fractals [17,18]. Fractals can be divided into two categories, i.e., random and deterministic fractals [19]. The most distinct features of fractals are self-similarity and fractional dimensions. The effective noninteger Hausdorff dimensionality of a fractal is defined by $d_f = \ln a/\ln b$ [20,21], where a denotes how many fractal structures of the previous generation are needed to build the next generation, and b represents the ratio of the geometrical size for two adjacent generations. Very recently, the study of the topological phenomena in fractal lattices has begun to attract attention [22–28]. Because the fractal lattice lacks translational symmetry and Bloch's theorem is not applicable anymore, the topological invariants thus should be determined in real space [29–31]. Owing to the existence of the multiple internal edges and corners, the fractal geometries can support fascinating topologically protected inner edge states and corner states, which have been demonstrated experimentally in acoustic and photonic systems [32–34].

In magnetic systems, spin waves (or magnons) and magnetic textures (which can also be viewed as bound states of infinite magnons) are two important excitations. By utilizing the nonlinear effect, Wu *et al.* [35] and Richardson *et al.* [36] experimentally observed a spin-wave fractal in the frequency domain when the power of the input microwave exceeds a critical value. Additionally, it has been shown that the spin-wave spectra can be tuned over a wide range of frequencies in magnetic deterministic fractals, such as Sierpiński carpets [37,38] and triangles [39,40]. On the other hand, over the past decade, various topological states in magnon- and texture-based crystals with integral dimensions have been reported, for example, the first-order TIs (FOTIs) [41–44], HOTIs [45–48], and topological semimetals [49–52]. However, the exciting combination of magnetic fractals and topological physics is yet to be explored. One can expect that magnetic fractal geometry can be used to localize topologically protected spin waves (or texture oscillations), which are particularly helpful for designing magnonic devices with robust multimode transmission channels.

In this paper, we study the topological properties of a fractal lattice based on magnetic textures. We take a Sierpiński carpet as an example to demonstrate the principle. The vortex is considered a typical magnetic texture to show the exotic fractal higher-order topological states. By solving Thiele's equation, we obtain the band structure of the magnetic texture fractal lattice. The phase diagram of the system is derived by evaluating the real-space quadrupole moment, from which we conclude that, when $d_1/d_2 > 1.5$ (<1.5), the system is in second-order topological (trivial) phase. Here, d_1 and d_2

*Contact author: yan@uestc.edu.cn

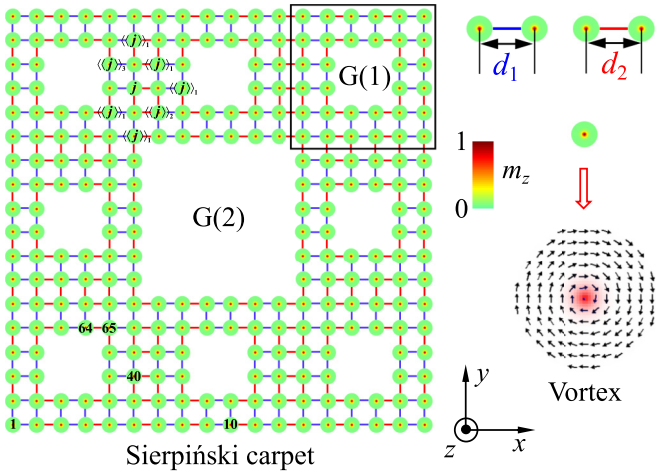

FIG. 1. Illustration of the Sierpiński carpet array of magnetic vortices. G(n) ($n = 1, 2, 3, ...$) denotes the nth generation fractal lattice. d_1 and d_2 represent the alternating geometric lengths. The inset plots the micromagnetic structure of a single vortex with topological charge $Q = +\frac{1}{2}$.

denote the alternating lengths between neighboring vortices, as shown in Fig. 1. Interestingly, when the system is in the HOTI phase, we discover three different topologically protected corner states with the oscillations confined at outer or inner corners. Our model mimics the two-dimensional Su-Schrieffer-Heeger (SSH) model of higher-order topology, as discussed in other systems [53–55]. We also perform micromagnetic simulations to confirm theoretical predictions with good agreement. Our results show that magnetic texture fractal lattices have potential applications for providing abundant topological modes in information processing, which should greatly promote the development of topological spintronics.

II. MODEL

In deterministic fractals, a Sierpiński carpet is one of the key structures, which has been widely considered for discussing topological phenomena [28,33,34]. In this paper, we focus on the second-generation Sierpiński carpet consisting of magnetic vortices, as shown in Fig. 1. For an nth-generation lattice, the total number of vortices is $N = 4 \times 8^n$. The corresponding Hausdorff dimensionality can be calculated as $d_f = \ln 8/\ln 3 \approx 1.893$, which does not depend on the value of the generation.

The collective dynamics of the vortex lattice can be characterized by the massless Thiele equation [56,57]:

$$G\hat{z} \times \frac{d\mathbf{U}_j}{dt} + \mathbf{F}_j = 0. \tag{1}$$

Here, $G = -4\pi Q w M_s/\gamma$ is the gyroscopic coefficient, $Q = \frac{1}{4\pi}\iint dxdy\mathbf{m} \cdot (\frac{\partial \mathbf{m}}{\partial x} \times \frac{\partial \mathbf{m}}{\partial y})$ is the topological charge, $\mathbf{m}$ is the unit vector of the local magnetic moment, w is the thickness of the nanodisk, M_s is the saturation magnetization, and γ is the gyromagnetic ratio. The displacement of the vortex core from the equilibrium position can be expressed as $\mathbf{U}_j = \mathbf{R}_j - \mathbf{R}_j^0$. The conservative force $\mathbf{F}_j = -\partial W/\partial \mathbf{U}_j$, with W being the total potential energy (including the contributions from the confinement of disk boundary and the interaction between nearest-neighbor vortices): $W = \sum_j K\mathbf{U}_j^2/2 + \sum_{j\neq k} U_{jk}/2$, where $U_{jk} = I_\parallel U_j^\parallel U_k^\parallel - I_\perp U_j^\perp U_k^\perp$ [58,59]. Here, K is the spring constant, and $I_\parallel$ and $I_\perp$ are the longitudinal and transverse coupling constants, respectively.

Imposing $\mathbf{U}_j = (u_j, v_j)$ and $\psi_j = u_j + iv_j$, and adopting the rotating wave approximation, Eq. (1) can be recast as [60]

$$\begin{aligned} -i\dot{\psi}_j = &\left(\omega_0 - \frac{\xi_1^2 + \xi_2^2}{\omega_0}\right)\psi_j + \sum_{k\in\langle j\rangle, l} \zeta_l \psi_k \\ &- \frac{\xi_1\xi_2}{2\omega_0} \sum_{s\in\langle\langle j\rangle\rangle_1} \exp(i2\bar{\theta}_{js})\psi_s \\ &- \frac{\xi_2^2}{2\omega_0} \sum_{s\in\langle\langle j\rangle\rangle_2} \exp(i2\bar{\theta}_{js})\psi_s \\ &- \frac{\xi_1^2}{2\omega_0} \sum_{s\in\langle\langle j\rangle\rangle_3} \exp(i2\bar{\theta}_{js})\psi_s, \end{aligned} \tag{2}$$

where $\omega_0 = K/|G|$, $\zeta_l = (I_{\parallel,l} - I_{\perp,l})/2|G|$, $\xi_l = (I_{\parallel,l} + I_{\perp,l})/2|G|$, $l = 1, 2$ denotes the different bond, $\bar{\theta}_{js}$ is the relative geometric angle, and $\langle j\rangle$ is the set of nearest neighbors of j. For any site j, there exist three different routes to couple next-nearest neighbor sites, i.e., $d_1 \to d_1$, $d_2 \to d_2$, and $d_1 \to d_2$ (or $d_2 \to d_1$) hoppings, which correspond to $\langle\langle j\rangle\rangle_3$, $\langle\langle j\rangle\rangle_2$, and $\langle\langle j\rangle\rangle_1$, respectively (see Fig. 1). By solving Eq. (2), one can obtain the spectra and eigenmodes of the vortex lattice. In this paper, we use the parameters of a Permalloy (Py) [61,62] nanodisk with thickness $w = 10$ nm and radius $r = 50$ nm. Then we get the gyrotropic frequency $\omega_0 = 2\pi \times 0.939$ GHz, gyroscopic coefficient $G = -3.0725 \times 10^{-13}$ J s rad^{-1} m^{-2}, and spring constant $K = 1.8128 \times 10^{-3}$ J m^{-2} [10]. The explicit expressions for $I_\parallel$ and $I_\perp$ as a function of d have been determined in our previous work [10]: $I_\parallel = \mu_0 M_s^2 r(-1.72064 \times 10^{-4} + 4.13166 \times 10^{-2}/d^3 - 0.24639/d^5 + 1.21066/d^7 - 1.81836/d^9)$ and $I_\perp = \mu_0 M_s^2 r(5.43158\times10^{-4} - 4.34685\times10^{-2}/d^3 + 1.23778/d^5 - 6.48907/d^7 + 13.6422/d^9)$, where d is the dimensionless distance parameter normalized by the nanodisk radius r, and μ_0 is the vacuum permeability.

III. CORNER STATES IN FRACTAL LATTICES

The spectrum of the second-generation Sierpiński carpet (see Fig. 1) as a function of d_1/d_2 is depicted in Fig. 2(a). We can see that the system supports several different bands, indicating abundant states emerging in this structure. When d_1/d_2 is greater than a critical value, an isolated band with fixed frequency $\omega/2\pi = 0.939$ GHz (gyrotropic frequency of a single vortex) appears, which is the typical feature for corner states [marked by the purple arrow in Fig. 2(a)]. To analyze localized states in detail, we choose the geometric parameters $d_1 = 194$ nm and $d_2 = 106$ nm ($d_1/d_2 = 1.83$), with the eigenfrequencies shown in Fig. 2(b). By plotting the spatial distribution of the eigenfunctions, we identify five different states: bulk state, edge state, outer corner state, type-I inner corner state (with oscillations spreading to all three vortices at the inner corner), and type-II inner corner state (only two nonadjacent vortices oscillate), marked by black, blue, red, magenta, and cyan dots

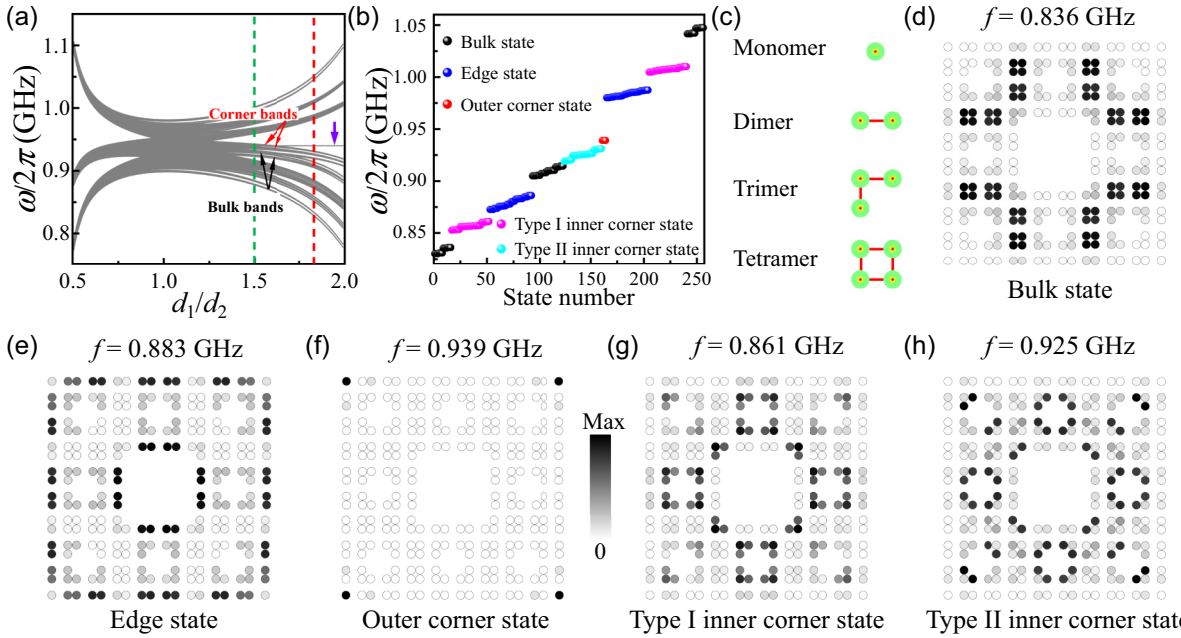

FIG. 2. (a) The eigenfrequencies of the second generation Sierpiński carpet lattice of magnetic vortices for different values of d_1/d_2. Here, we fix $d_1 + d_2 = 6r$. (b) The eigenfrequencies of the system with $d_1/d_2 = 1.83$ as marked by dashed red line in (a). (c) Four different basic elements of Sierpiński carpet lattice when $d_1 \to \infty$. The spatial distribution of vortex oscillations for the (d) bulk, (e) edge, (f) outer corner, (g) type-I inner corner, and (h) type-II inner corner states.

in Fig. 2(b), respectively. The emergence of these states can be intuitively understood by considering the zero-correlation length limit, i.e., $d_1 \to \infty$ ($d_1 = 1.83d_2$ and $d_1 \to \infty$ are in the same topological phase, as discussed below). In this case, the system has four different basic elements: monomer, dimer, trimer, and tetramer, as shown in Fig. 2(c). Therefore, when the vortex oscillations are localized to monomer position, the lattice exhibits the outer corner state [see Fig. 2(f)]. If the oscillations are confined to dimer and tetramer positions, the system, however, supports the edge state [see Fig. 2(e)] and bulk state [see Fig. 2(d)], respectively. Interestingly, when the trimer positions dominate the oscillations, the vortex lattice shows two different inner corner states, i.e., type I [see Fig. 2(g)] and type II [see Fig. 2(h)]. This characteristic is reminiscent of the corner states emerging in obtuse-angled corners of a breathing honeycomb lattice [47].

Since the fractal lattice lacks translational symmetry, the topological invariant should be calculated in real space to characterize HOTIs. One of the appropriate topological invariants is the real-space quadrupole moment Q_{xy}, which is given by [30,31,34]

$$Q_{xy} = -\frac{i}{2\pi}\ln[\det(S)] \mod 1,$$
$$S_{n,m} = V_n^* \exp\left(\frac{i2\pi\hat{x}\hat{y}}{l_x l_y}\right) V_m, \tag{3}$$

where V_n is the nth wave function [by solving Eq. (2)] of the fractal lattice with periodic boundary conditions in both x and y directions, $\hat{x}$ ($\hat{y}$) is the position operator along the x (y) direction, and l_x (l_y) is the length of the lattice in the x (y) axis. Interestingly, we note that the second-generation Sierpiński carpet can be constructed from a square lattice by removing nine subsquares (see Fig. 1). Comparing the band structure of an infinite square lattice [60] with Fig. 2(b), one finds that the corner states of the fractal lattice mainly emerge between the third and fourth energy bands. We therefore consider $\frac{3}{4}$ band filling (i.e., the bands below the outer corner states are filled) to calculate the real-space quadrupole moment. Figure 3(a) plots the dependence of Q_{xy} on the ratio d_1/d_2 with red dots. For comparison, the topological invariant Z_4 Berry phase of the square lattice is also plotted with black dots. We can clearly see that Q_{xy} is quantized to 0 when $d_1/d_2 < 1.5$ and to 0.5 otherwise, indicating that $d_1/d_2 = 1.5$ is the phase

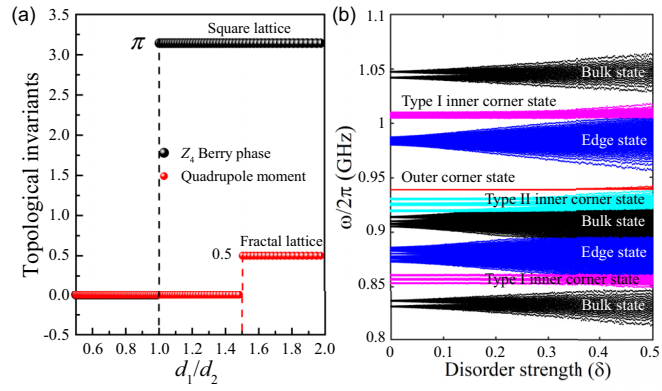

FIG. 3. (a) Dependence of topological invariants Z_4 Berry phase (for two-dimensional breathing square lattice) and real-space quadrupole moment (for Sierpiński carpet fractal lattice) on the ratio d_1/d_2. (b) The eigenfrequencies of collective vortex oscillations for fractal lattice under different disorder strengths. Here, the value of d_1/d_2 is fixed to 1.83.

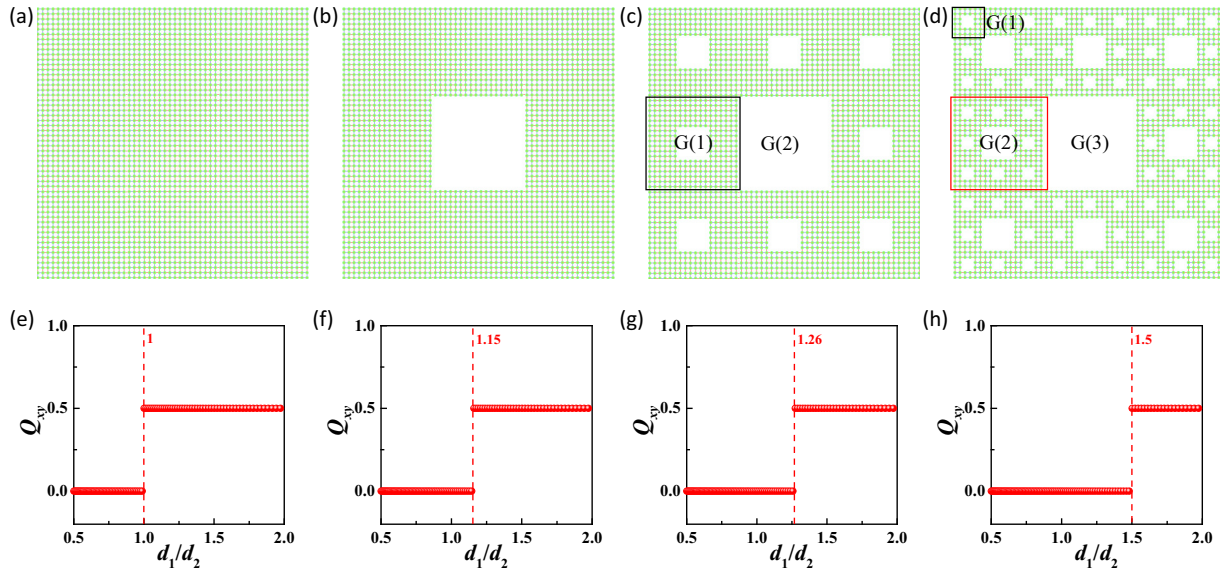

FIG. 4. (a)–(d) Illustrations of vortex lattices with more and more voids. (e)–(h) Corresponding topological invariant quadrupole moments.

transition point separating the trivial and higher-order topological phases.

Additionally, we identify that the quadrupole moment is origin independent, which is like the case in an electronic system [27]. It is well known that the phase transition point is $d_1/d_2 = 1$ for a square lattice. In such a case, we can say that the nontrivial standard region is squeezed from a square lattice $[d_1/d_2 \in (1, +\infty)]$ to fractal cases $[d_1/d_2 \in (1.5, +\infty)]$. This squeezing phenomenon can be explained by the spatial translational symmetry breaking resulting from the voids. We further verify that the more severe the spatial translational symmetry breaking, the larger the value of topological phase transition point d_1/d_2, as shown in Fig. 4. One can naturally expect such a case: If the spatial translational symmetry is totally broken, the system cannot support any topological phases, i.e., phase transition point $d_1/d_2 \to \infty$. Moreover, we find that the phase transition point is independent of the number of the carpet generations [see Figs. 3(a) and 4(h)], which can be qualitatively understood by the fact that, because of the self-similarity, different generations have the same degree of spatial translational symmetry breaking [34]. Moreover, we must point out that the first (second)-generation Sierpiński carpets emerging in Figs. 4(c) and 4(d) are different due to the distinct duty cycle.

For conventional periodic lattices, at the topological phase transition point, the band gap closing/opening can be clearly observed in momentum space, while we can only obtain the real-space spectrum for fractals owing to the fact that Bloch's theorem fails to describe the bands. The real-space spectrum exhibits great width for different bands (bulk, edge, and corner). Although it is difficult to identify the gap closing/opening at a topological phase transition point, we can find that the corner and bulk [red and black arrows in Fig. 2(a)] bands begin to separate in frequency when $d_1/d_2 = 1.5$, which corresponds to the topological phase transition point.

To further examine whether the corner states emerging in Fig. 2(b) are topologically protected, we calculate the eigenfrequencies of the fractal vortex lattice under different disorder strengths, with the result being plotted in Fig. 3(b). Here, the disorders are introduced by supposing that the coupling parameters ζ and ξ suffer a random change, i.e., $\zeta \to \zeta(1 + \delta Z)$ and $\xi \to \xi(1 + \delta Z)$, where δ denotes the strength of the disorder, and Z is a random number uniformly distributed between -1 and 1, which apply to all vortices. We average the numerical results for 100 realizations to avoid the error from a single calculation. From Fig. 3(b), we can see that both frequencies of the outer and inner corner states are robust for moderate disorder strength. Interestingly, we find the critical value of disorder strength for shifting the frequencies of the outer corner states is larger than those for the inner corner states, which indicates that the outer corner state has stronger topological stability than the inner ones.

Additionally, if we introduce random empty sites in the square lattice, localized states around the empty sites may appear. However, these local modes are not protected by symmetry and therefore are trivial. As a result, the critical difference between a fractal and a conventional square lattice with random empty sites is that the corner states are topologically protected in fractals while not in a conventional square lattice with random empty sites.

Our model can also be mapped to the tight-binding model with the following Hamiltonian:

$$\begin{aligned}\mathcal{H} = &\sum_j \left(\omega_0 - \frac{\xi_1^2 + \xi_2^2}{\omega_0}\right)\psi_j^*\psi_j + \zeta \sum_{\langle jk\rangle} \psi_j^*\psi_k \\ &- \frac{\xi_1\xi_2}{2\omega_0} \sum_{\langle\langle jk\rangle\rangle_1} \exp(i2\bar{\theta}_{jk})\psi_j^*\psi_k \\ &- \frac{\xi_2^2}{2\omega_0} \sum_{\langle\langle jk\rangle\rangle_2} \exp(i2\bar{\theta}_{jk})\psi_j^*\psi_k \\ &- \frac{\xi_1^2}{2\omega_0} \sum_{\langle\langle jk\rangle\rangle_3} \exp(i2\bar{\theta}_{jk})\psi_j^*\psi_k + \text{c.c.} \end{aligned} \tag{4}$$

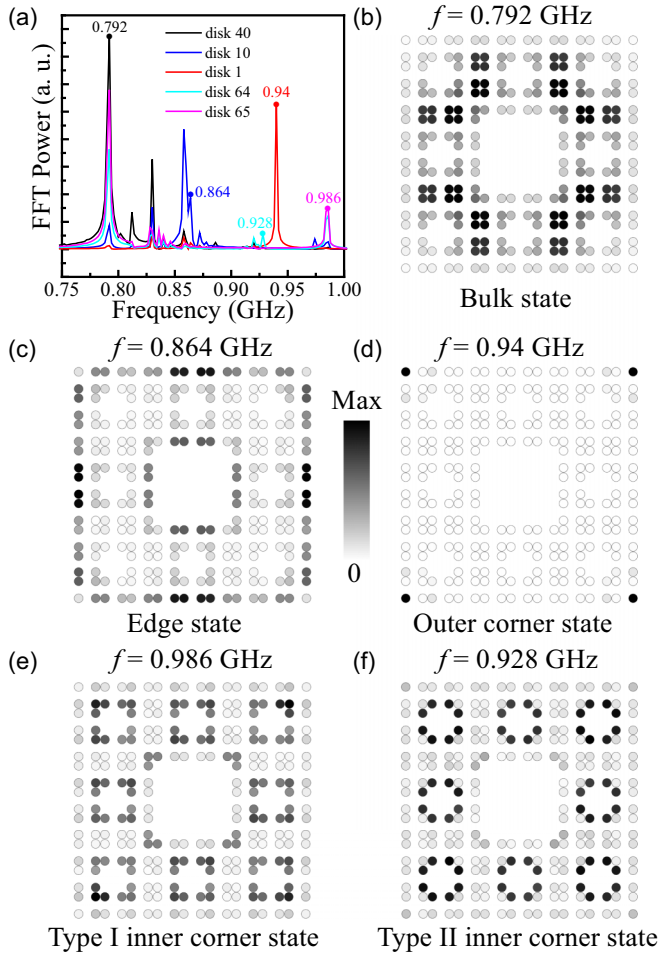

FIG. 5. (a) The temporal Fourier spectra of the vortex oscillations at different positions as marked in Fig. 1. (b)–(f) The spatial distribution of fast Fourier transform (FFT) intensity for different modes.

Comparing with the two-dimensional SSH model [53–55], our Hamiltonian contains an extra on-site term $\sum_j[\omega_0 - (\xi_1^2 + \xi_2^2)/\omega_0]\psi_j^*\psi_j$, which breaks the chiral symmetry. As a result, the corner and bulk states are spectrally separated in our model, while for the SSH system, these states spectrally overlap with each other. Remarkably, this feature provides advantages to distinguish different modes in our system. Additionally, the mechanism for generating higher-order topology is analog to the SSH model. The higher-order topological states emerging in our model are protected by C_4 symmetry.

IV. MICROMAGNETIC SIMULATIONS

To verify the theoretical predictions about the fractal higher-order topological states, we perform full micromagnetic simulations [63]. The second-generation Sierpiński carpet array consisting of 256 identical magnetic vortices is considered, as shown in Fig. 1. We compute the temporal fast Fourier transform (FFT) spectrum of the vortex oscillations at different positions, labeled 1, 10, 40, 64, and 65 in Fig. 1. Figure 5(a) plots the numerical results, with black, blue, red, cyan, and magenta curves representing the positions of bulk (No. 40), edge (No. 10), outer corner (No. 1), inner corner 1 (No. 64), and inner corner 2 (No. 65) bands, respectively. From Fig. 5(a), we find that, near the frequency of 0.94 GHz, the outer corner band has a very strong peak, while other bands do not, which is an obvious feature of an outer corner state with oscillations confined only at four outer corners. The frequency range supporting other states can be obtained through a similar principle. The spatial distributions of the FFT intensity with representative frequencies are plotted in Figs. 5(b)–5(f) to visualize the characteristics of different modes. We can identify the bulk, edge, outer corner, and inner corner states of both type-I and II with vortex oscillation localized at the tetramer [see Fig. 5(b)], dimer [see Fig. 5(c)], monomer [see Fig. 5(d)], and trimer [see Figs. 5(e) and 5(f)], respectively. Interestingly, due to the absence of dimers in the smallest vacant squares, the type-I inner corner states exhibit exotic characteristics with oscillation spreading over all vortices in these regions. These results agree well with the theoretical calculations presented in Fig. 2.

V. DISCUSSION AND CONCLUSION

From an experimental perspective, the fabrication and detection of HOTIs in magnetic texture fractal are fully within the reach of current technology. On the one hand, artificial fractals of magnetic nanodisks (it is convenient to obtain vortex or skyrmion states when appropriate parameters are chosen) can be created with electron-beam lithography [65,66] or x-ray illumination [67]. On the other hand, the nanometer-scale magnetic texture positions can be tracked by using a biased conductive scanning nanoscale tip [68] or ultrafast Lorentz microscopy technique [69]. The magnetic texture arrays thus provide an ideal platform for studying fractal topology. In addition, higher-order topological states emerging in magnetic texture fractal lattices are expected to have a lot of potential applications for information processing. For example, the topologically protected inner corner states in fractal geometry provide massive oscillation sources, which can be used to design multifrequency robust nano-oscillators. Additionally, by constructing fractal lattice with different generations, one can achieve the localization of magnetic texture oscillations (information) at desired positions for display application.

Comparing with a two-dimensional square lattice with translational symmetry, our model exhibits several unusual properties, apart from some similarities. Firstly, the Sierpiński carpet is constructed by cutting numerous subsquares from the two-dimensional square lattice. Therefore, the unit cell contains four sites both for fractal and square lattices. Secondly, due to the existence of multiple internal edges and corners, the fractal lattices have more edge and corner states than conventional square lattices. Thirdly, when considering the second-order topological phase, there only exist three basic elements for square lattices, i.e., monomer, dimer, and tetramer; however, the fractal lattice has an additional trimer. As a result, the fractal lattices can support exotic inner corner states, while square lattices cannot. Finally, both corner states emerging in fractal and square lattices are protected by fourfold rotation symmetry.

In this paper, we only focus on the Sierpiński carpet array, while other fractal lattices, for example, Sierpiński gaskets [28,32] and Koch curves [22], should support exotic localized topological modes too. In addition to the magnetic vortex, there exist several other magnetic textures, such as skyrmions [70,71], magnetic bubbles [72,73], and domain walls [74,75]. The study of fractal TIs based on these magnetic textures is an appealing research topic, from which one can expect the multichannel propagation of magnons and topologically protected multimode oscillators. To accurately describe the dynamics of a vortex, the higher-order terms, like the mass term and non-Newtonian gyration term, should be added to Thiele's equation [10,43]. In such a case, the system then may provide more topologically protected outer and inner corner states, which is also an interesting issue for study.

To summarize, we have investigated the higher-order topological phases in a second-generation Sierpiński carpet of magnetic vortices. The band structures of the collective vortex oscillations were calculated by solving Thiele's equation. We found that the fractal lattice can exhibit one type of outer corner state and two different types of inner corner states under proper geometric conditions. By evaluating the real-space quadrupole moment as the topological invariant, we obtain the full phase diagram. We showed that both outer and inner corner states are topologically robust against moderate disorder. Full micromagnetic simulations were performed to verify the theoretical predictions with great agreement. Our findings provide important theoretical reference to investigating the in-gap states in magnetic texture based fractals, which also represent a crucial step for combining fractal and topological physics.

ACKNOWLEDGMENTS

We thank Z. Wang and X. S. Wang for helpful discussions. This paper was supported by the National Key R&D Program under Contract No. 2022YFA1402802 and the National Natural Science Foundation of China (NSFC; Grants No. 12074057 and No. 12374103). Z.-X.L. acknowledges financial support from the NSFC (Grant No. 11904048) and the Natural Science Foundation of Hunan Province of China (Grant No. 2023JJ40694).

[1] M. Z. Hasan and C. L. Kane, Colloquium: Topological insulators, Rev. Mod. Phys. **82**, 3045 (2010).
[2] X.-L. Qi and S.-C. Zhang, Topological insulators and superconductors, Rev. Mod. Phys. **83**, 1057 (2011).
[3] Z.-X. Li, Y. Cao, and P. Yan, *Topology in Collective Magnetization Dynamics* (IOP, Bristol, 2023).
[4] W. A. Benalcazar, B. A. Bernevig, and T. L. Hughes, Quantized electric multipole insulators, Science **357**, 61 (2017).
[5] F. Schindler, A. M. Cook, M. G. Vergniory, Z. Wang, S. S. P. Parkin, B. A. Bernevig, and T. Neupert, Higher-order topological insulators, Sci. Adv. **4**, eaat0346 (2018).
[6] A. E. Hassan, F. K. Kunst, A. Moritz, G. Andler, E. J. Bergholtz, and M. Bourennane, Corner states of light in photonic waveguides, Nat. Photon. **13**, 697 (2019).
[7] H. Xue, Y. Yang, F. Gao, Y. Chong, and B. Zhang, Acoustic higher-order topological insulator on a kagome lattice, Nat. Mater. **18**, 108 (2019).
[8] S. Imhof, C. Berger, F. Bayer, J. Brehm, L. W. Molenkamp, T. Kiessling, F. Schindler, C. H. Lee, M. Greiter, T. Neupert *et al.*, Topolectrical-circuit realization of topological corner modes, Nat. Phys. **14**, 925 (2018).
[9] H. Fan, B. Xia, L. Tong, S. Zheng, and D. Yu, Elastic higher-order topological insulator with topologically protected corner states, Phys. Rev. Lett. **122**, 204301 (2019).
[10] Z.-X. Li, Y. Cao, P. Yan, and X. R. Wang, Higher-order topological solitonic insulators, npj Comput. Mater. **5**, 107 (2019).
[11] Y. Hatsugai, Chern number and edge states in the integer quantum Hall effect, Phys. Rev. Lett. **71**, 3697 (1993).
[12] W. A. Benalcazar, B. A. Bernevig, and T. L. Hughes, Electric multipole moments, topological multipole moment pumping, and chiral hinge states in crystalline insulators, Phys. Rev. B **96**, 245115 (2017).
[13] B. Xie, H.-X. Wang, X. Zhang, P. Zhan, J.-H. Jiang, M. Lu, and Y. Chen, Higher-order band topology, Nat. Rev. Phys. **3**, 520 (2021).
[14] Z.-X. Li, Y. Cao, and P. Yan, Topological insulators and semimetals in classical magnetic systems, Phys. Rep. **915**, 1 (2021).
[15] L. Bindi, P. J. Steinhardt, N. Yao, and P. J. Lu, Natural quasicrystals, Science **324**, 1306 (2009).
[16] E. Maciá-Barber, *Quasicrystals, Fundamentals and Applications*, (CRC Press, Boca Raton, 2020).
[17] B. Mandelbrot, How long is the coast of Britain? Statistical self-similarity and fractional dimension, Science **156**, 636 (1967).
[18] T. Nakayama and K. Yakubo, *Fractal Concepts in Condensed Matter Physics* (Springer-Verlag, Berlin, 2003).
[19] B. B. Mandelbrot, *Fractals: Form, Chance, and Dimension* (Freeman, San Francisco, 1977).
[20] F. Hausdorff, Dimension und äußeres Maß, Math. Ann. **79**, 157 (1918).
[21] C. McMullen, The Hausdorff dimension of general Sierpiński carpets, Nagoya Math. J. **96**, 1 (1984).
[22] Z. G. Song, Y. Y. Zhang, and S. S. Li, The topological insulator in a fractal space, Appl. Phys. Lett. **104**, 233106 (2014).
[23] M. Brzezińska, A. M. Cook, and T. Neupert, Topology in the Sierpiński-Hofstadter problem, Phys. Rev. B **98**, 205116 (2018).
[24] S. Pai and A. Prem, Topological states on fractal lattices, Phys. Rev. B **100**, 155135 (2019).
[25] M. Fremling, M. V. Hooft, C. M. Smith, and L. Fritz, Existence of robust edge currents in Sierpiński fractals, Phys. Rev. Res. **2**, 013044 (2020).
[26] C. Liu, Y. Zhou, G. Wang, Y. Yin, C. Li, H. Huang, D. Guan, Y. Li, S. Wang, H. Zheng *et al.*, Sierpiński structure and electronic topology in Bi thin films on InSb(111)B Surfaces, Phys. Rev. Lett. **126**, 176102 (2021).
[27] S. Manna, S. Nandy, and B. Roy, Higher-order topological phases on fractal lattices, Phys. Rev. B **105**, L201301 (2022).
[28] B. Ren, Y. V. Kartashov, L. J. Maczewsky, M. S. Kirsch, H. Wang, A. Szameit, M. Heinrich, and Y. Zhang, Theory of

nonlinear corner states in photonic fractal lattices, Nanophoton. **12**, 3829 (2023).
[29] R. Resta, Quantum-mechanical position operator in extended systems, Phys. Rev. Lett. **80**, 1800 (1998).
[30] W. A. Wheeler, L. K. Wagner, and T. L. Hughes, Many-body electric multipole operators in extended systems, Phys. Rev. B **100**, 245135 (2019).
[31] B. Kang, K. Shiozaki, and G. Y. Cho, Many-body order parameters for multipoles in solids, Phys. Rev. B **100**, 245134 (2019).
[32] T. Biesenthal, L. J. Maczewsky, Z. Yang, M. Kremer, M. Segev, A. Szameit, and M. Heinrich, Fractal photonic topological insulators, Science **376**, 1114 (2022).
[33] S. Zheng, X. Man, Z.-L. Kong, Z.-K. Lin, G. Duan, N. Chen, D. Yu, J.-H. Jiang, and B. Xia, Observation of fractal higher-order topological states in acoustic metamaterials, Sci. Bull. **67**, 2069 (2022).
[34] J. Li, Q. Mo, J.-H. Jiang, and Z. Yang, Higher-order topological phase in an acoustic fractal lattice, Sci. Bull. **67**, 2040 (2022).
[35] M. Wu, B. A. Kalinikos, L. D. Carr, and C. E. Patton, Observation of spin-wave soliton fractals in magnetic film active feedback rings, Phys. Rev. Lett. **96**, 187202 (2006).
[36] D. Richardson, B. A. Kalinikos, L. D. Carr, and M. Wu, Spontaneous exact spin-wave fractals in magnonic crystals, Phys. Rev. Lett. **121**, 107204 (2018).
[37] P. Monceau and J.-C. S. Lévy, Spin waves in deterministic fractals, Phys. Lett. A **374**, 1872 (2010).
[38] C. Swoboda, M. Martens, and G. Meier, Control of spin-wave excitations in deterministic fractals, Phys. Rev. B **91**, 064416 (2015).
[39] J. Zhou, M. Zelent, S. Parchenko, Z. Luo, V. Scagnoli, M. Krawczyk, L. J. Heyderman, and S. Saha, Precessional dynamics of geometrically scaled magnetostatic spin waves in two-dimensional magnonic fractals, Phys. Rev. B **105**, 174415 (2022).
[40] R. Mehta, M. Moalic, M. Krawczyk, and S. Saha, Tunability of spin-wave spectra in a 2D triangular shaped magnonic fractals, J. Phys.: Condens. Matter **35**, 324002 (2023).
[41] A. Mook, J. Henk, and I. Mertig, Edge states in topological magnon insulators, Phys. Rev. B **90**, 024412 (2014).
[42] X. S. Wang, Y. Su, and X. R. Wang, Topologically protected unidirectional edge spin waves and beam splitter, Phys. Rev. B **95**, 014435 (2017).
[43] Z.-X. Li, C. Wang, Y. Cao, and P. Yan, Edge states in a two-dimensional honeycomb lattice of massive magnetic skyrmions, Phys. Rev. B **98**, 180407(R) (2018).
[44] Z.-X. Li, Z. Wang, Y. Cao, H. W. Zhang, and P. Yan, Robust edge states in magnetic soliton racetrack, Phys. Rev. B **103**, 054438 (2021).
[45] T. Hirosawa, S. A. Díaz, J. Klinovaja, and D. Loss, Magnonic quadrupole topological insulator in antiskyrmion crystals, Phys. Rev. Lett. **125**, 207204 (2020).
[46] A. Mook, S. A. Díaz, J. Klinovaja, and D. Loss, Chiral hinge magnons in second-order topological magnon insulators, Phys. Rev. B **104**, 024406 (2021).
[47] Z.-X. Li, Y. Cao, X. R. Wang, and P. Yan, Symmetry-protected zero modes in metamaterials based on topological spin texture, Phys. Rev. Appl. **13**, 064058 (2020).
[48] Z.-X. Li, Z. Wang, Z. Zhang, Y. Cao, and P. Yan, Third-order topological insulator in three-dimensional lattice of magnetic vortices, Phys. Rev. B **103**, 214442 (2021).
[49] J. Fransson, A. M. Black-Schaffer, and A. V. Balatsky, Magnon Dirac materials, Phys. Rev. B **94**, 075401 (2016).
[50] Y. Su, X. S. Wang, and X. R. Wang, Magnonic Weyl semimetal and chiral anomaly in pyrochlore ferromagnets, Phys. Rev. B **95**, 224403 (2017).
[51] A. Mook, J. Henk, and I. Mertig, Magnon nodal-line semimetals and drumhead surface states in anisotropic pyrochlore ferromagnets, Phys. Rev. B **95**, 014418 (2017).
[52] Z.-X. Li, X. S. Wang, L. Song, Y. Cao, and P. Yan, Type-II Weyl excitation in vortex arrays, Phys. Rev. Appl. **17**, 024054 (2022).
[53] F. Liu and K. Wakabayashi, Novel topological phase with a zero Berry curvature, Phys. Rev. Lett. **118**, 076803 (2017).
[54] M. Kim and J. Rho, Topological edge and corner states in a two-dimensional photonic Su-Schrieffer-Heeger lattice, Nanophoton. **9**, 3227 (2020).
[55] B.-Y. Xie, H.-F. Wang, H.-X. Wang, X.-Y. Zhu, J.-H. Jiang, M.-H. Lu, and Y.-F. Chen, Second-order photonic topological insulator with corner states, Phys. Rev. B **98**, 205147 (2018).
[56] A. A. Thiele, Steady-state motion of magnetic domains, Phys. Rev. Lett. **30**, 230 (1973).
[57] S. K. Kim and Y. Tserkovnyak, Chiral edge mode in the coupled dynamics of magnetic solitons in a honeycomb lattice, Phys. Rev. Lett. **119**, 077204 (2017).
[58] J. Shibata, K. Shigeto, and Y. Otani, Dynamics of magnetostatically coupled vortices in magnetic nanodisks, Phys. Rev. B **67**, 224404 (2003).
[59] J. Shibata and Y. Otani, Magnetic vortex dynamics in a two-dimensional square lattice of ferromagnetic nanodisks, Phys. Rev. B **70**, 012404 (2004).
[60] Z.-X. Li, Y. Cao, X. R. Wang, and P. Yan, Second-order topological solitonic insulator in a breathing square lattice of magnetic vortices, Phys. Rev. B **101**, 184404 (2020).
[61] M. W. Yoo, J. Lee, and S. K. Kim, Radial-spin-wave-modeassisted vortex-core magnetization reversals, Appl. Phys. Lett. **100**, 172413 (2012).
[62] S. Velten, R. Streubel, A. Farhan, N. Kent, M.-Y. Im, A. Scholl, S. Dhuey, C. Behncke, G. Meier, and P. Fischer, Vortex circulation patterns in planar microdisk arrays, Appl. Phys. Lett. **110**, 262406 (2017).
[63] The parameters used in the simulations are the same as those for the theoretical determinations in Fig. 2(b): the saturation magnetization $M_s = 0.86 \times 10^6$ A/m, the exchange stiffness $A = 1.3 \times 10^{-11}$ J/m, and the Gilbert damping constant $\alpha = 10^{-4}$ (to observe the vortex oscillations clearly). We use the micromagnetic software MUMAX3 [64] to simulate the collective dynamics of vortex lattice. The cell size is chosen to be $2 \times 2 \times 10$ nm^3. To obtain the spectrum of the vortex oscillations in the vicinity of the gyrotropic mode (here, the gyrotropic frequency of a single vortex is 939 MHz), we apply a sinc-function magnetic field $H(t) = H_0 \sin[2\pi f(t - t_0)]/[2\pi f(t - t_0)]$ along the x direction, with $H_0 = 10$ mT, $f = 5$ GHz, and $t_0 = 1$ ns, over the whole system for 500 ns. The position of vortex cores $\mathbf{R}_j = (R_{j,x}, R_{j,y})$ for all nanodisks are recorded every 200 ps. Here, $R_{j,x}$ and $R_{j,y}$ are calculated through $R_{j,x} = \iint x|m_z|^2 dxdy / \iint |m_z|^2 dxdy$ and $R_{j,y} = \iint y|m_z|^2 dxdy / \iint |m_z|^2 dxdy$, where the integral region is confined in the jth nanodisk.

[64] A. Vansteenkiste, J. Leliaert, M. Dvornik, M. Helsen, F. Garcia-Sanchez, and B. V. Waeyenberge, The design and verification of MUMAX3, AIP Adv. **4**, 107133 (2014).

[65] C. Behncke, M. Hänze, C. F. Adolff, M. Weigand, and G. Meier, Band structure engineering of two-dimensional magnonic vortex crystals, Phys. Rev. B **91**, 224417 (2015).

[66] L. Sun, R. X. Cao, B. F. Miao, Z. Feng, B. You, D. Wu, W. Zhang, A. Hu, and H. F. Ding, Creating an artificial two-dimensional skyrmion crystal by nanopatterning, Phys. Rev. Lett. **110**, 167201 (2013).

[67] Y. Guang, I. Bykova, Y. Liu, G. Yu, E. Goering, M. Weigand, J. Gräfe, S. K. Kim, J. Zhang, H. Zhang *et al.*, Creating zero-field skyrmions in exchange-biased multilayers through x-ray illumination, Nat. Commun. **11**, 949 (2020).

[68] D. Yu, C. Sui, D. Schulz, J. Berakdar, and C. Jia, Nanoscale near-field steering of magnetic vortices, Phys. Rev. Appl. **16**, 034032 (2021).

[69] M. Möller, J. H. Gaida, S. Schäfer, and C. Ropers, Few-nm tracking of current-driven magnetic vortex orbits using ultrafast Lorentz microscopy, Commun. Phys. **3**, 36 (2020).

[70] S. Mühlbauer, B. Binz, F. Jonietz, C. Pfleiderer, A. Rosch, A. Neubauer, R. Georgii, and P. Böni, Skyrmion lattice in a chiral magnet, Science **323**, 915 (2009).

[71] W. Jiang, P. Upadhyaya, W. Zhang, G. Yu, M. B. Jungfleisch, F. Y. Fradin, J. E. Pearson, Y. Tserkovnyak, K. L. Wang, O. Heinonen *et al.*, Blowing magnetic skyrmion bubbles, Science **349**, 283 (2015).

[72] K.-W. Moon, B. S. Chun, W. Kim, Z. Q. Qiu, and C. Hwang, Control of skyrmion magnetic bubble gyration, Phys. Rev. B **89**, 064413 (2014).

[73] I. Makhfudz, B. Krüger, and O. Tchernyshyov, Inertia and chiral edge modes of a skyrmion magnetic bubble, Phys. Rev. Lett. **109**, 217201 (2012).

[74] D. Atkinson, D. A. Allwood, G. Xiong, M. D. Cooke, C. C. Faulkner, and R. P. Cowburn, Magnetic domain-wall dynamics in a submicrometre ferromagnetic structure, Nat. Mater. **2**, 85 (2003).

[75] G. Catalan, J. Seidel, R. Ramesh, and J. F. Scott, Domain wall nanoelectronics, Rev. Mod. Phys. **84**, 119 (2012).